Revista de Metalurgia
January-March 2021, 57 (1), e187
ISSN-L: 0034-8570
https://doi.org/10.3989/revmetalm.187

Microstructure analysis of welding fume of low and medium carbon steels

Bekir Güney*

Karamanoğlu Mehmetbey University, Vocational School of Technical Sciences, Yunus Emre Yerleşkesi, 70100 Karaman, Turkey

(*Corresponding author: guneyb@kmu.edu.tr)

Submitted: 2 May 2020; Accepted: 20 January 2021; Available On-line: 7 April 2021

ABSTRACT: In this study, the sample of welding fume was obtained from low and medium carbon steels and the electrodes used in welding. The microstructures of the particles were analysed using scanning electron microscopy (SEM), energy dispersive spectrometer (EDS), X-ray diffractometer (XRD) and fourier transform infrared spectrometer (FTIR). In the experiments; Be, O, F, Fe, Si, Cl, K, Ca, Ti, V, Cr, Mn were found to be atomically more than 1%. Based on this finding, it is revealed that the structure is composed mainly of oxides such as Fe_2O_3, Fe_3O_4, MnO_2, TiO_2, SiO_2, $Fe_3Mn_3O_8$, $FeMn_2O_4$, BeO, CrO. It was also found with XRD analysis that the elements which were found to beatomically less 1% formed oxide phases. Because oxidized structures threaten the environment and human health, it has been experimentally found that the metals and heavy metals emitted by welding fumes still keep polluting and threatening the environment.

KEYWORDS: Human healty; Microstructure; Pollution; Welding fume

Citation/Citar como: Güney, B. (2021). “Microstructure analysis of welding fume of low and medium carbon steels”. *Rev. Metal.* 57(1): e187. https://doi.org/10.3989/revmetalm.187

RESUMEN*: Análisis de la microestructura de humos de soldadura de aceros de bajo y medio contenido de carbon.* En este estudio, la muestra de humo de soldadura se obtuvo a partir de aceros de bajo y medio carbono y los electrodos utilizados en la soldadura. Las microestructuras de las partículas se analizaron mediante microscopía electrónica de barrido (SEM), espectrómetro de dispersión de energía (EDS), difractómetro de rayos X (XRD) y espectrómetro de infrarrojos por transformada de Fourier (FTIR). En los experimentos se encontró que los elementos Be, O, F, Fe, Si, Cl, K, Ca, Ti, V, Cr, Mn tenían contenidos atómicos superiores al 1%. Con base en este hallazgo, se revela que la estructura está constituida principalmente por óxidos tipos Fe_2O_3, Fe_3O_4, MnO_2, TiO_2, SiO_2, $Fe_3Mn_3O_8$, $FeMn_2O_4$, BeO, CrO. También se encontró mediante análisis XRD que los elementos con contenidos inferiores al 1% atómico se encontraban también asociados a fases en forma de óxidos. Debido a que las estructuras oxidadas amenazan el medio ambiente y la salud humana, se ha descubierto experimentalmente que los metales emitidos por los humos de soldadura siguen contaminando y amenazando el medio ambiente.

PALABRAS CLAVE: Contaminación; Humos de soldadura; Microestructura; Salud humana

ORCID ID: Bekir Güney (https://orcid.org/0000-0001-9764-9313)

1. INTRODUCTION

Metals have excellent mechanical properties compared to other materials in terms of hardness, toughness and strength (Shackelford *et al.*, 2016). In industrial applications, the bonding of these metals is usually obtained by a welding technique. During welding, it is necessary to have a base metal, additional metal and a heat source (Turan *et al.*, 2011). The welding arc forming is a process of accumulating an electric arc between welding electrode and base material, melting the metals at the joining (Cary and Helzer, 2005; Erden *et al.,* 2018).

According to the science of physics, welding arc occurs when electrons emitted from the cathode portion bombard the anode with a high speed as the electric current passes from one conductive metal to another. This bombardment causes a strong rise in temperature since it causes the ionization of the neutral molecules at the end of the impact (Anık, 2001). The temperature above 4000 ºC in the arc (Palmer and Eaton, 2001) allows the metals to melt and thus to bond (Howden, *et al.*, 1988). Each material is a potential source of fume when heated to high temperatures. Welding fumes are produced as a result of metallurgical reactions at high temperatures. Some of the metal components which are heated well above the electrode boiling degree are released as gases by burning or evaporating into the atmosphere. The vaporous components are condensed again to become ultra-fine fume particles smaller than 100 nm, which are light enough to fly in the air and small enough to breathe.

Chemical composition of welding fumes depends on the welding technique used, welding parameters, melting, welding metal and welding electrode which has a composition of metal (Berlinger *et al.*, 2019). When welding, welding fumes, gases and electromagnetic energy (radiation) are usually released in indoor areas.

Welding fumes are caused by melting and evaporation of metal wire electrodes or dust during joining or coating of metals. A variety of metallic and non-metallic elements and compounds are present in the fume composition (Sowards *et al.*, 2010), including, metallic oxides, silicates and fluorides, as well as complex mixtures of heavy metal contaminants such as cadmium, aluminium, chromium, copper and lead (Rana *et al.*, 2019). Some of these particles vent into the atmosphere and some of them hang in the air for a while and then accumulate on the ground as a result of condensation, air movement, gravity or atomic interactions.

Inhalation of toxic metals and metalloids poses a risk to workers' health in many industries. Today, among these health-damaging factors, great importance is given to the toxic effects caused by welding fumes (Flechsig, 1988). It is estimated that more than one hundred million workers worldwide work as welders and more than three million employees weld at certain intervals as part of their work (McNeilly *et al.*, 2004).

Arc welding procedures emit solid particles and gases that may have adverse health-related effects following inhalation, including cardiovascular (Sjogren *et al.*, 2006), neurological (Fored *et al.*, 2006) respiratory signs and symptoms. Therefore, it may cause environmental and health problems (Lighty *et al.*, 2000; Antonini, 2003; Donaldson *et al.*, 2005; Jenkins and Eagar 2005a; Oberdörster *et al.*, 2005). Welding fume has toxicity which may be hazardous to human health if inhaled or swallowed in pure form. Metal oxides exhibiting toxic characteristics contain alloying elements which can be dangerous in this sense (Jenkins and Eagar, 2005a).

Previous works have reported some specific chemical composition of welding (Ehrman *et al.*, 1999; Jenkins and Eagar, 2005a; Jenkins and Eagar, 2005b; Sowards *et al.*, 2010; Golbabaei and Khadem, 2015; Stebounova *et al.*, 2018). However, there is still need of a study involving comprehensive analysis of chemical composition of welding fume in order to have better understanding on possible adverse health effects, and have create better preventive and safety strategies. Accordingly, in this study, the microstructure of low and medium carbon steels and welding particles obtained from electrodes used in their welding were characterized by using SEM, EDS, XRD and FTIR techniques.

2. MATERIALS AND METHODS

2.1. Welding fume collection

The welding fume sample was obtained from the fume of electrodes used in low and medium carbon steels and their electric arc welding since carbon steels are the most commonly used materials in the world (Golbabaei and Khadem, 2015). These particles were deposited by vacuuming to a ceramic filter at the room temperature. The studies were carried out in the Material Characterization Laboratory at Karamanoğlu Mehmetbey University, Scientific and Technological Researches Application and Research Center.

2.2. Micro structure analysis

The fume particles were aspirated at room temperature and collected in a ceramic filter. Microstructure analyses were performed with a field emission SEM (HITACHI SU5000) equipped with EDS operating at 10 kV. IR spectroscopy (Bruker Vertex 70 ATR) was used to measure the FTIR spectrum of the sample. The data were collected by vibration frequencies at 4000-400 cm^{-1}scanning range at 4 cm^{-1} spectral resolution. X-ray diffraction phase analysis was performed with a Bruker D8 ADVACE with DAVINCI XRD (Cu-Kα radiation, λ = 1,5406 Å in the range 10° ≤ 2θ ≤ 90° operated at 40 kV and 40 mA) with secondary beam graphite monochromator. The phase analyses were characterized by the data obtained from the Diffract EVA software and the International Centre for Diffraction Data (ICCD).

3. RESULTS AND DISCUSSION

3.1. Characterization by XRD

The composition of the welding fume particles comprises different structures due to the cooling mechanism and the agglomerated method. X-ray diffraction studies revealed that approximately 90% of the fume is crystal structure (Fig. 1). Since the source fume particles are composed of many elements and molecules according to the results of the EDS and FTIR analyses, many peaks of XRD phase analysis were obtained (Fig. 1). According to EDS analysis, there were many elements in the structure. X-ray diffraction analysis revealed that different compounds had strong peaks at the same point. The peak in the same range indicated the presence of more than one compound. The peaks of the compounds given in Table 1, were the strongest matches.

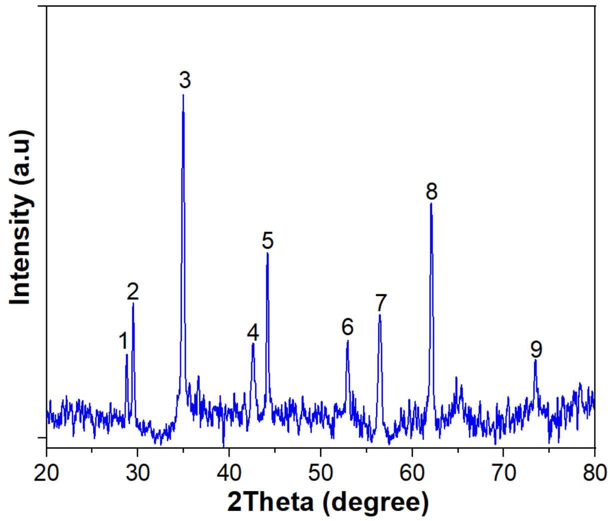

Figure 1. X- ray diffraction spectrum of welding fume.

Table 1. XRD diffraction spectra of welding fume with strong peaks

Name	Formula	Crystal System	Peak Number
Zinc Manganese Iron Oxide	$ZnMnFeO_4$	Cubic	2, 3, 5, 6, 7
Copper Iron Nickel Zinc Oxide	$Cu_{0.1}Fe_{1.9}Ni_{0.65}Zn_{0.35}O_4$	Cubic	2, 3, 4, 6, 7, 8
Iron Manganese Oxide	$Fe_3Mn_3O_8$	Cubic	2, 3, 4, 6, 7, 8
Manganese Iron Titanium Oxide	$(FeMn)_2TiO_3$	Rhombohedral	3, 6
Iron Manganese Oxide	$FeMn_2O_4$	Cubic	2, 3, 4, 6, 7, 8, 9
Manganese Iron Zinc Oxide	$Mn_{0.09}Fe_{0.08}Zn_{1.83}O_4$	Cubic	2, 3, 4, 6, 7, 8, 9
Zinc Manganese Iron Oxide	$Zn_2Mn_8Fe_2O_4$	Cubic	2, 3, 4, 6, 7, 8, 9
Zinc Manganese Iron Oxide	$Zn_4Mn_6Fe_2O_4$	Cubic	2, 3, 4, 6, 7, 8, 9
Zinc Manganese Iron Oxide	$Zn_6Mn_4Fe_2O_4$	Cubic	2, 3, 4, 6, 7, 8, 9
Zinc Manganese Iron Oxide	$Zn_9MnFe_2O_4$	Cubic	2, 3, 4, 6, 7, 8, 9
Zinc Manganese Iron Oxide	$ZnMnFe_3O_8$	Tetragonal	2, 3, 4, 6, 7, 8, 9
Magnetite	Fe_3O_4	Orthorhombic	1, 2, 3, 4, 6, 7, 8, 9
Fayalite, Manganoan	$(FeMn)_2SiO_4$	Orthorhombic	3, 9
Hematite	Fe_2O_3	Tetragonal	1, 2, 3, 4, 6, 7, 8
Iron Oxide	FeO	Orthorhombic	2, 3
Aluminum Oxide	Al_2O_3	Orthorhombic	2, 3, 4
Berylium Oxide	BeO	Hexagonal	5
Chromium Oxide	Cr_2O_3	Rhombohedral	5
Copper Magnesium	Mg_2Cu	Orthorhombic	3, 4, 5
Periclase	MgO	Cubic	4, 8, 9
Manganese Oxide	MnO_2	Hexagonal	4, 7, 9
Sodium Oxide	Na_2O_2	Hexagonal	1, 3, 4
Nickel Titanium Oxide	Ni_2Ti_4O	Cubic	3, 7, 8
Silicon Oxide	SiO_2	Monoclinic	1, 3
Titanium Oxide	TiO_2	Cubic	3, 7
Zinc Titanium Oxide	Zn_2TiO_4	Cubic	2, 3, 4, 6, 7, 8, 9
Zirconium Oxide	ZrO_2	Rhombohedral	2, 3

Since welding fumes consist of ultra-fine particles, these structures were essentially shapeless. The structures of the phases obtained from the XRD analysis given in Table 1 were composed of different crystal lattice structures as reported in previous studies (Ehrman *et al.*, 1999; Stebounova *et al.*, 2018). During the condensation of these particles, separate molecules may get together to form different phases in a single structure. In some structures, other oxide shells could be found around the iron oxide core. Therefore, particle structures are generally heterogeneous (Jenkins and Eagar, 2005b).

Welding fume is a product of high temperature. It is possible that a large number of elements or molecules present in the body can form very different compounds at these elevated temperatures. Based on this, information on the compounds giving peaks in the XRD analysis of the fume material was given in Table 1. When Table 2 was examined, it is very difficult to analyze the structure in detail due to the elements which can be included in the structure uncontrolled from the atmosphere depending on the chemical content of the materials used in forming the welding arc or due to the effect of high temperature. However, it is possible to say that Fe and Mn-based structures are predominant. It is understood from the XRD analyses that intermetallics such as NiAl, TiNi are formed in the structure due to high temperature. When the peaks obtained by XRD were evaluated together with EDS and FTIR analyses, Be element BeO, K element K_2O, Ca element CaO, V element $V1_6O_3$, Ti element Zn_2TiO_4, Ni_2Ti_4O, W element W_3O_8, and Cr element CrO are available in the structure forming Si element SiO_2. X-Ray diffraction analysis showed that the dominant phase in the whole fume was highly correlated with Fe_3O_4 in the magnetite structure and Fe_2O_3 in the hematite structure which gives strong peaks (Jenkins and Eagar, 2005b). Other possible structures were MgO, K_2CO_3, Na_2CO_3 and $MnFe_2O_4$. The results of the analysis reveal that welding fume contains various oxides in very complex structures and different combinations.

3.2. Characterization by scanning electron microscopy

The images of such structures were difficult to analyses with SEM. The small welding fume particles formed larger spherical agglomerated particles by the cooling mechanism from vapour state. These agglomerates appear on the micrographs

Table 2. Atomic quantities of elements detected in welding fume according to EDS analysis

Elements	Atomic%								
	Fig. 2	Fig. 3a			Fig. 3b			Fig. 3c	Fig. 3d
		Point 1	Point 2	Point 3	Point 1	Point 2	Point 3		
Be	2,05	3,52	1,87	1,34	3,36	3,47	3,84	2,15	3,01
Fe	30,48	13,21	28,41	30,73	31,27	55,01	41,51	34,89	47,50
Co	0,29	0,19	0,13	0,40	0,23	0,02	0,04	0,27	0,39
Ni	0,17	0,06	0,06	0,09	0,05	0,14	0,26	0,49	0,02
Cu	0,34	0,10	0,12	0,01	0,18	0,57	0,26	0,20	0,28
Zn	0,02	0,23	0,14	0,13	0,25	0,24	0,28	0,55	0,63
Na	1,53	0,15	0,12	0,38	1,47	0,53	0,28	0,24	0,58
Mg	1,42	1,07	0,52	0,13	1,71	1,15	0,97	1,41	1,00
Br	1,86	2,09	0,42	0,28	2,05	0,45	1,17	0,83	0,56
Al	0,04	0,25	0,07	0,06	0,05	0,05	0,06	0,05	0,05
Si	11,22	16,35	3,24	1,91	19,67	4,26	3,48	8,56	1,97
P	0,57	0,75	0,79	0,20	0,56	0,10	1,68	6,51	5,70
Zr	0,36	0,48	0,15	0,02	0,11	0,60	0,08	0,02	0,62
Nb	0,50	0,04	0,45	0,21	0,36	0,48	0,99	0,64	
Mo	0,63	0,23	0,80	0,40	0,47	0,62	0,87	0,44	0,30
S	0,38	0,02	0,10	0,05	0,02	0,05	0,06	0,05	1,69
Cl	1,99	1,11	1,25	0,69	1,67	1,39	2,08	1,52	2,06
Pd	1,03	0,73	1,38	0,77	0,79	1,00	1,66	1,16	0,95
K	5,63	4,50	3,97	3,89	6,97	3,11	3,31	3,00	3,43
Ca	10,13	5,51	24,05	16,48	7,02	3,61	4,43	7,90	2,46
Ti	9,17	29,94	12,01	7,64	5,03	5,26	8,55	6,85	2,76
V	3,46	3,27	4,43	4,71	3,81	5,24	6,63	3,26	5,98
Cr	5,93	4,31	4,70	11,32	3,99	4,69	11,54	9,09	7,66
Mn	9,76	11,87	10,83	18,14	8,91	7,65	5,92	9,91	10,30

as foam or finely mixed hair (Fig. 2) (Jenkins and Eagar, 2005b). However, larger particles can also be produced by spattering from the welding arc. Large particles were composed of Al, Si, K, Na, F and water-soluble compounds, while small particles were predominantly composed of heavy metals such as Fe, Ni, Mo, Mn, Cr and their oxides.

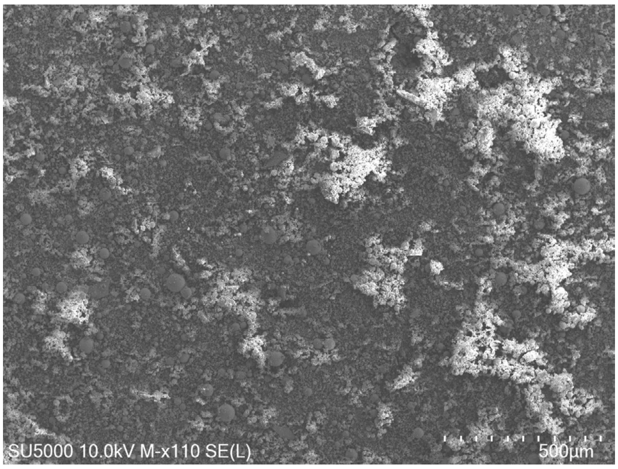

Figure 2. SEM micrograph of 110x magnification taken from welding fume surface.

The welding fume was shown in Table 1, where the metallic elements which were present in the composition are represented by different % atomic ratios in the form of compounds. The elements in the structure such as Be, Ca, Cl, Cr, Fe, Mn, K, Si, Ti and V were found to be atomically higher than 1% due to the welded material and the structure of the electrode. In addition, when the results of XRD and EDS analyses were examined together, the elements such as Al, Br, Co, Mg, Mo, Na, Nb, Ni, P, Pd, S, Zn, and Zr were found to be less than 1% or in trace amount. Since the temperature reached at the source is about 4000 °C (Palmer and Eaton, 2001) all elements in the structure are almost gaseous. During the gas condensation of welding fumes, the amount of O added from the atmosphere to the composition is high in concentration. Metallic nanostructure particles tend to compound rapidly with O. This tendency leads to the formation of high amounts of metal oxides, the main element of the fume concentration.

When the SEM micrograph in 110x magnification was examined in Fig. 2, regarding fume morphology, the structure consisting of oxide deposits and predominantly spherical particles on the surface is striking. When the EDS analysis of Fig. 2 was examined in Table 2, it is seen that the elements Mn, Fe, Ti, Ca, Si, V, Cr, Cl, K and Be were atomically high in the structure.

Figure 3a shows three different types of particles in the 2.000x magnification micrograph. Spherical particles are predominantly seen in the micrograph. These were the particles flaking during condensation and are the most commonly observed particles at each stage. The other was common, although a much lower amount of isolated spherical particles is present. The third was the irregularly shaped particles with the lowest density. When the EDS analysis conducted in point 1of Fig. 3a was examined in Table 2, it is seen that Mn, Br, Ti, Ca, Si, V, Cr, K and Be elements were atomically high. When the EDS analysis of point 2 in Fig. 3a was examined in Table 2, it is seen that the elements Ti, Mn, Si, Cl, Cr, Ca, K, V, Be and Pd were also atomically high.

When the EDS analysis of point 3 in Fig. 3 is examined in Table 2, it is seen that the elements Ti, Mn, Si, Cr, Ca, K, V and Be were atomically high. The micrograph of spherical particles constituting the majority of the fume morphology was given in Fig. 3b in 5.000x magnification. When the EDS analysis of point 1 of Fig. 3b is examined in Table 2, it is seen that the elements Mn, Fe, Ti, Ca, Si, V, Cr, K and Be were atomically high. When the EDS analysis of point 2 of Fig. 3b is examined in Table 2, it is seen that the elements Mn, Fe, Ti, Ca, Si, V, Cr, K and Be were atomically high. When the EDS analysis of point 3 of Fig. 3b is examined in Table 2, it is seen that the elements Mn, Fe, Ti, Ca, Si, V, Cr, Cl, K and Be were atomically high. When the EDS analysis of Fig. 3b in Table 2 is examined, it was found that the elements Mn, Fe, Ti, Ca, Si, V, Cr, K were atomically high. The micrograph of spherical particles of different sizes and particles which tend to agglomerate is given in Fig. 3c at 10.000x magnification. The spherical particle size is shown in Fig. 3d in 20.000x magnification. When the EDS analysis of the surface of the micrograph was analysed in Table 2, it was found that the elements Fe, Si, P, Cl, K, Ca, Ti, V, Cr, and Mn were atomically high. Particle morphology needs to be considered as it determines the surface area of a part and the aerodynamic diameter of the particles. A pellet has a much larger surface area than the individual spherical particle having the same cross-section. These agglomerates also have different aerodynamic properties that can affect the degree to which they can be inhaled (Sowards *et al.*, 2008). When EDS analysis was evaluated in general, it was found that Be, Fe, Si, Cl, K, Ca, Ti, V, Cr, and Mn elements were found to be high in each point examined. When evaluated together with FTIR and XRD analyses, it reveals that the structure is composed of the molecules and compounds belonging to the elements that are detected more atomically.

Smaller particles are subjected to higher degrees of overcooling in the first fume vapor. This causes the formation of primary particles in the fumes produced during welding. Thus, metallic particles in the chemical elements found in the welding are condensed and nucleated. The elements that are

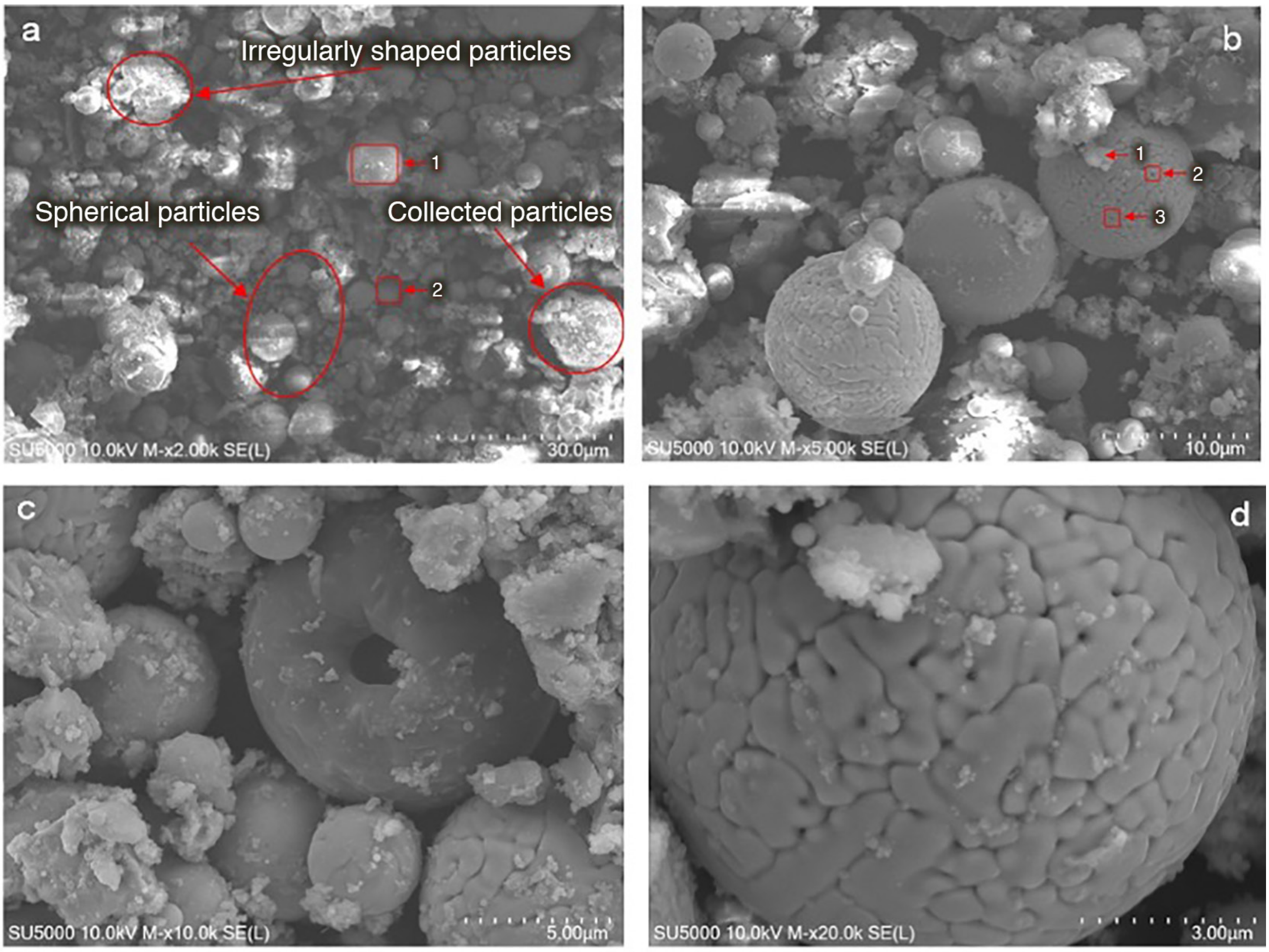

Figure 3. SEM micrograph of welding fume surface with a magnification of: a) 2.000x, b) 5.000x, c) 10.000x, and d) 20.000x.

lighter in the fume may not be involved in nucleation and may be vented into the atmosphere. This resulted in the formation of higher amounts of elements such as Be, Fe, Si, Cl, K, Ca, Ti, V, Cr and Mn in the source fume composition (Sowards *et al.*, 2010). Other structures consist of nanoparticles having multiple oxidation states, which are formed as amorphous or single nanoparticles or agglomerates which have been able to achieve compounding capacity during condensation.

3.3. Characterization by FTIR

FTIR measurements were performed to investigate the bonds of functional free and complex molecules in the source fume (Fig. 4). According to the EDS analysis of the welding fume sample, the bonding structures of the metallic-based elements which are more than 1% by weight are examined. According to the peak values shown in Fig. 4; 3296, peaks in the band range of 2921 cm^{-1} (Ehrman *et al.*, 1999; Jenkins *et al.*, 2005a; Jenkins and Eagar, 2005b; Wang *et al.*, 2006; Chen and He, 2008; Sowards

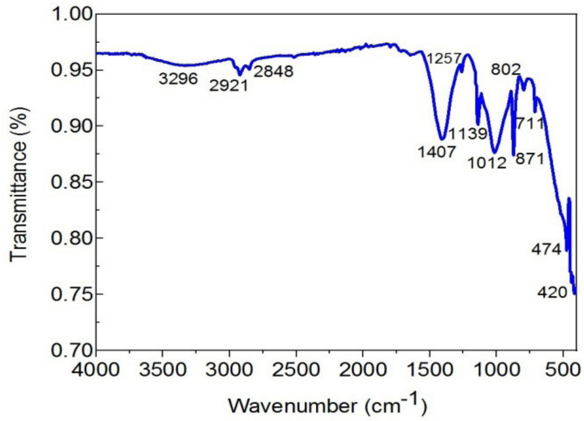

Figure 4. Characterization of welding fume particles FTIR spectrum.

et al., 2008; Sevilla and Fuertes, 2009; Gibot and Vidal, 2010; Saikia and Parthasarathy, 2010; Zheng *et al.*, 2010; Vaculikova *et al.*, 2011; Basu *et al.*, 2011; Farzaneh and Najafi, 2011; Lin *et al.*, 2012; Abdullah *et al.*, 2014; Jamal *et al.*, 2014; Golbabaei and Khadem, 2015; Naushad *et al.*, 2015; Diko *et al.*, 2016; Sahai *et al.*, 2016; Benykhlef *et al.*, 2016; Yi *et al.*, 2018; Ge *et al.*, 2019; Habtemariam *et al.*, 2019; Bahah *et al.*, 2019; Abinaya *et al.*, 2019; Alias *et al.*, 2019; Altunal *et al.*, 2019; Boroń *et al.*, 2019; Reddy *et al.*, 2019; Karthik *et al.*, 2019; Karunathilaka *et al.*, 2019; Kono *et al.*, 2019; Mohammadi *et al.*, 2019; Ponmudi *et al.*2019; Scaccia *et al.*, 2019; Wang *et al.*, 2019a; Wang *et al.*, 2019b; Yang *et al.*, 2019), indicate O-H bonding in the structure. This indicates the presence of an H_2O molecule. Peaks in the band range of 1012 and 420 cm^{-1} were obtained due to the tension of the metal oxide bonds. The FTIR peaks of the elements in the source fume obtained according to EDS analysis were consistent with the literature Al-O (Jamal *et al.*, 2014; Benykhlef *et al.*, 2016; Yi *et al.*, 2018), Be-O (Altunal *et al.*, 2019), Br-O (Naushad *et al.*, 2015), C-O, CaO and CH (Scaccia *et al.*, 2019), Cd-O (Karthik *et al.*, 2019), Cl-O (Wang *et al.*, 2019a), Co-O (Gibot and Vidal, 2010), Cr-O (Basu *et al.*, 2011; Farzaneh and Najafi, 2011; Abdullah *et al.*, 2014), Cu-O (Zheng *et al.*, 2010; Sahai *et al.*, 2016; Ponmudi *et al.*, 2019), Fe-O (Abdullah *et al.*, 2014; Golbabaei and Khadem, 2015), Mn-O (Chen and He, 2008; Sevilla and Fuertes, 2009; Lin *et al.*, 2012), Mo-O (Abinaya *et al.*, 2019), N-O (Boroń *et al.*, 2019; Yang *et al.*, 2019), P-O (Kono *et al.*, 2019), Pd-O (Reddy *et al.*, 2019), S-O (Yang *et al.*, 2019), Si-O (Saikia and Parthasarathy, 2010; Vaculikova *et al.*, 2011; Diko *et al.*, 2016; Bahah *et al.*, 2019; Mohammadi *et al.*, 2019), Ti-O (Jamal *et al.*, 2014), V-O (Wang *et al.*, 2006; Habtemariam *et al.*, 2019), Zr-O (Wang *et al.*, 2019b) metal oxides and oxide structures in different structures because metal oxides generally exhibit peaks below 1000 cm^{-1}, which may be caused by inter-atomic vibrations (Lagashetty *et al.*, 2007).

Welded metal and additional metal have a rich chemical composition. During joining, a certain amount of this rich structure burns or evaporates and thus forms welding fumes. Welding fumes contain very different structures by its nature. 1139, 1257, 1407, 2848 and 2921 cm^{-1} peaks obtained from FTIR analysis were Al-O (Jamal *et al.*, 2014; Benykhlef *et al.*, 2016; Yi *et al.*, 2018), Cl-O (Wang *et al.*, 2019a), Co-O (Gibot and Vidal, 2010), C-H and CC (Scaccia *et al.*, 2019), C-F (Karunathilaka *et al.*, 2019), C-Br (Nicasio-Collazo *et al.*, 2019), N-H (Oswald *et al.*, 2019), C-N (Panja and Ghosh, 2019), Fe-O and Fe_2O_4 (Abdullah *et al.*, 2014; Golbabaei and Khadem, 2015), F_2O_3 (Oberdörster *et al.*, 2005), Mn-O (Jamal *et al.*, 2014; Alias *et al.*, 2019), N-O (Boroń *et al.*, 2019; Yang *et al.*, 2019), P-O (Kono *et al.*, 2019), Pd-O (Reddy *et al.*, 2019), Si-O (Saikia and Parthasarathy, 2010; Vaculikova *et al.*, 2011; Diko *et al.*, 2016; Bahah *et al.*, 2019; Mohammadi *et al.*, 2019) functional due to the fact that stretching of bonds of functional groups has increased.

4. CONCLUSIONS

- In this study, the molecular structure, compound structure and crystal structure of the elements which are formed after melting, evaporation and combustion were investigated. With this study; Be, Fe, Si, Cl, K, Ca, Ti, V, Cr and Mn were found to be more than 1% of the total composition in the welding fume. Based on this finding, it is concluded that the structure is mainly composed of oxides such as Fe_2O_3, Fe_3O_4, MnO_2, TiO_2, SiO_2, $Fe_3Mn_3O_8$, $FeMn_2O_4$, BeO and CrO. Welding fume is released into the atmosphere as a high-temperature product. Therefore, it has been experimentally explained that combinations of oxidized structures characterizing welding fume have complex morphology and chemical properties. In addition, it was determined by SEM micrographs that other nano-sized particles were found to be amorphous.
- These properties have potential effects on toxicity mechanisms. However, previous studies have experimentally showed that metals and heavy metals emitted by welding fumes still pollute the environment.
- Therefore, it can be clearly stated that these materials are vented into the atmosphere and threaten the environment and human health because the fume produced during the welding process contains many different oxides and elements (Stockmann-Juvala *et al.*, 2013; Stebounova *et al.*, 2018; McCarrick, *et al.*, 2019).
- The data obtained in this study provide important information for understanding the effects of welding fumes on health and environment. More efforts should be made to reduce the emission values emitted by welding fumes to the environment.

ACKNOWLEDGMENTS

I would like to thank Mehmetbey University, Scientific and Technological Research Application and Research Center, Material Characterization Laboratory staff, to whom I have received assistance in conducting this study.

REFERENCES

Abdullah, M.M., Rajab, F.M., Al-Abbas, S.M. (2014). Structural and optical characterization of Cr_2O_3 nanostructures: Evaluation of its dielectric properties. *AIP Advances* 4 (2), 027121. https://doi.org/10.1063/1.4867012.

Abinaya, M., Saravanakumar, K., Jeyabharathi, E., Muthuraj, V. (2019). Synthesis and Characterization of 1D-MoO_3 Nanorods Using Abutilon indicum Extract for the Photoreduction of Hexavalent Chromium. *J. Inorg. Organomet. Polym. Mater.* 29 (1), 101-110. https://doi.org/10.1007/s10904-018-0970-0.

Alias, S.S., Harun, Z., Azhar, F.H., Yusof, K.N., Jamalludin, M.R., Hubadillah, S.K., Basri, S.N., Al-Harthi, M.A. (2019). Enhancing the performance of a hybrid porous polysulfone membrane impregnated with green Ag/AgO additives derived from the Parkia speciosa. *Vacuum* 163, 301-311. https://doi.org/10.1016/j.vacuum.2019.02.034.
Anık, S. (1991). *Methods and Equipment, Welding Technique Handbook*. Gedik Foundation Publications, pp. 1-50.
Antonini, J.M. (2003). Health effects of welding. *Critical reviews in toxicology* 33 (1), 61-103. https://doi.org/10.1080/713611032.
Altunal, V., Guckan, V., Ozdemir, A., Can, N., Yegingil, Z. (2019). Luminescence characteristics of Al-and Ca-doped BeO obtained via a sol-gel method. *J. Phys. Chem. Solids* 131, 230-242. https://doi.org/10.1016/j.jpcs.2019.04.003.
Bahah, S., Nacef, S., Chebli, D., Bouguettoucha, A., Djellouli, B. (2019). A New Highly Efficient Algerian Clay for the Removal of Heavy Metals of Cu (II) and Pb (II) from Aqueous Solutions: Characterization, Fractal, Kinetics, and Isotherm Analysis. *Arab. J. Sci. Eng.* 45 (1), 205-218. https://doi.org/10.1007/s13369-019-03985-6.
Basu, M., Sinha, A.K., Pradhan, M., Sarkar, S., Negishi, Y., Pal, T. (2011). Fabrication and functionalization of CuO for tuning superhydrophobic thin film and cotton wool. *J. Phys. Chem. C* 115 (43), 20953-20963. https://doi.org/10.1021/jp206178x.
Benykhlef, S., Bekhoukh, A., Berenguer, R., Benyoucef, A., Morallon, E. (2016). PANI-derived polymer/Al_2O_3 nanocomposites: synthesis, characterization, and electrochemical studies. *Colloid Polym. Sci.* 294 (12), 1877-1885. https://doi.org/10.1007/s00396-016-3955-y.
Berlinger, B., Weinbruch, S., Ellingsen, D.G., Zibarev, E., Chashchin, V., Chashchin, M., Thomassen, Y. (2019). On the bio-accessibility of 14 elements in welding fumes. *Environ. Sci.- Proc. Imp.* 21 (3), 497-505. https://doi.org/10.1039/c8em00425k.
Boroń, P., Rutkowska, M., Gil, B., Marszałek, B., Chmielarz, L., Dzwigaj, S. (2019). Experimental Evidence of the Mechanism of Selective Catalytic Reduction of NO with NH_3 over Fe-Containing BEA Zeolites. *ChemSusChem* 12 (3), 692-705. https://doi.org/10.1002/cssc.201801883.
Cary, H.B., Helzer, S.C. (2005). *Welding, Modern Welding Technology*. Pearson Education, pp. 1-169.
Chen, H., He, J. (2008). Facile synthesis of monodisperse manganese oxide nanostructures and their application in water treatment. *J. Phys. Chem. C* 112 (45), 17540-17545. https://doi.org/10.1021/jp806160g.
Diko, M., Ekosse, G., Ogola, J. (2016). Fourier transform infrared spectroscopy and thermal analyses of kaolinitic clays from South Africa and Cameroon. *Acta Geodyn. Geomater.* 13 (2), 149-158. https://doi.org/10.13168/AGG.2015.0052.
Donaldson, K., Tran, L., Jimenez, L.A., Duffin, R., Newby, D.E., Mills, N., Stone, V. (2005). Combustion-derived nanoparticles: A review of their toxicology following inhalation exposure. *Part. Fibre Toxicol.* 2 (1), 1-14. https://doi.org/10.1186/1743-8977-2-10.
Erden, M.A., Gündüz, S., Çalıgülü, U., Boz, M. (2018). Tozaltı kaynak yöntemi ile birleştirilen alaşımsız ve hardoks çeliklerin mikroyapı ve sertlik özelliklerinin araştırılması. *Journal of the Faculty of Engineering and Architecture of Gazi University* 33 (1), 221-226.
Ehrman, S.H., Friedlander, S.K., Zachariah, M.R. (1999). Phase segregation in binary SiO_2/TiO_2 and SiO_2/Fe_2O_3 nanoparticle aerosols formed in a premixed flame. *J. Mater. Res.* 14 (12), 4551-4561. https://doi.org/10.1557/JMR.1999.0617.
Farzaneh, F., Najafi, M. (2011). Synthesis and characterization of Cr_2O_3 nanoparticles with triethanolamine in water under microwave irradiation. *J. Sci. I. R. Iran* 22 (4), 329-333.
Flechsig, R. (1988). What do we know today about welding-fume effects on the respiratory system?. *Ind. Health* 26 (2), 93-100. https://doi.org/10.2486/indhealth.26.93.
Fored, C.M., Fryzek, J.P., Brandt, L., Nise, G., Sjögren, B., McLaughlin, J.K., Ekbom, A. (2006). Parkinson's disease and other basal ganglia or movement disorders in a large nationwide cohort of Swedish welders. *Occup. Environ. Med.* 63 (2), 135-140. https://doi.org/10.1136/oem.2005.022921.
Ge, Y., Shen, W., Wang, X., Feng, H., Feng, L. (2019). Synthesis and bactericidal action of Fe_3O_4/AgO bifunctional magnetic-bactericidal nanocomposite. *Colloid Surface A* 563, 160-169. https://doi.org/10.1016/j.colsurfa.2018.11.063.
Gibot, P., Vidal, L. (2010). Original synthesis of chromium (III) oxide nanoparticles. *J. Eur. Ceram. Soc.* 30 (4), 911-915. https://doi.org/10.1016/j.jeurceramsoc.2009.09.019.
Golbabaei, F., Khadem, M. (2015). *Air pollution in welding processes - Assessment and control methods. In Current Air Quality Issues*. Chapter 2, In Tech, pp. 33-63.
Habtemariam, A.B., Kabtamu, D.M., Maaza, M. (2019). One-step hydrothermal synthesis and characterization of Mg/Mo co-doped VO_2 nanorods. *SN Appl. Sci.* 1 (5), 413. https://doi.org/10.1007/s42452-019-0448-x.
Howden, D.G., Desmeules, M.J.A., Saracci, R., Sprince, N.L., Herber, P.I. (1988). Respiratory hazards of welding: occupational exposure characterization. *Am. Rev. Respir. Dis* 138, 1047-1048.
Jamal, R., Osman, Y., Rahman, A., Ali, A., Zhang, Y., Abdiryim, T. (2014). Solid-state synthesis and photocatalytic activity of polyterthiophene derivatives/TiO_2 nanocomposites. *Materials* 7 (5), 3786-3801. https://doi.org/10.3390/ma7053786.
Jenkins, N.T., Eagar, T.W. (2005a). Fume formation from spatter oxidation during arc welding. *Sci. Technol. Weld. Joi.* 10 (5), 537-543. https://doi.org/10.1179/174329305X48310.
Jenkins, N.T., Eagar, T.W. (2005b). Chemical analysis of welding fume particles. *Weld. J.* 84 (6), 87-93.
Karthik, K., Dhanuskodi, S., Gobinath, C., Prabukumar, S., Sivaramakrishnan, S. (2019). Ultrasonic-assisted CdO-MgO nanocomposite for multifunctional applications. *Mater. Technol.* 34 (7), 403-414. https://doi.org/10.1080/10667857.2019.1574963.
Karunathilaka, S.R., Choi, S.H., Mossoba, M.M., Yakes, B.J., Brückner, L., Ellsworth, Z., Srigley, C.T. (2019). Rapid classification and quantification of marine oil omega-3 supplements using ATR-FTIR, FT-NIR and chemometrics. *J. Food Compos. Anal.* 77, 9-19. https://doi.org/10.1016/j.jfca.2018.12.009.
Kono, T., Watanabe, A., Kanno, T., Ootani, Y., Tamamura, R., Sakae, T., Okada, H. (2019). Second Order Differentiation Analysis of Micro FTIR Method Revealed the Variable Erosion Characteristics of Carbonated Soft Drink for the Individual Human Teeth Enamel. *J. Hard Tissue Biol.* 28 (1), 7-12. https://doi.org/10.2485/jhtb.28.7.
Lagashetty, A., Havanoor, V., Basavaraja, S., Balaji, S.D., Venkataraman, A. (2007). Microwave-assisted route for synthesis of nanosized metal oxides. *Sci. Technol. Adv. Mater.* 8 (6), 484-493. https://doi.org/10.1016/j.stam.2007.07.001.
Lighty, J.S., Veranth, J.M., Sarofim, A.F. (2000). Combustion aerosols: Factors governing their size and composition and implications to human health. *J. Air Waste Manage.* 50 (9), 1565-1618. https://doi.org/10.1080/10473289.2000.10464197.
Lin, C.C., Chen, C.J., Chiang, R.K. (2012). Facile synthesis of monodisperse MnO nanoparticles from bulk MnO. *J. Cryst. Growth* 338 (1), 152-156. https://doi.org/10.1016/j.jcrysgro.2011.10.022.
McCarrick, S., Wei, Z., Moelijker, N., Derr, R., Persson, K.A., Hendriks, G., Odnevall Wallinder, I., Hedberg, Y., Karlsson, H.L. (2019). High variability in toxicity of welding fume nanoparticles from stainless steel in lung cells and reporter cell lines: the role of particle reactivity and solubility. *Nanotoxicology* 13 (10), 1293-1309. https://doi.org/10.1080/17435390.2019.1650972.
McNeilly, J.D., Heal, M.R., Beverland, I.J., Howe, A., Gibson, M.D., Hibbs, L.R., MacNee, W., Donaldson, K., (2004). Soluble transition metals cause the pro-inflammatory effects of welding fumes in vitro. *Toxicol. Appl. Pharm.* 196 (1), 95-107. https://doi.org/10.1016/j.taap.2003.11.021.
Mohammadi, M., Khorrami, M.K., Ghasemzadeh, H. (2019). ATR-FTIR spectroscopy and chemometric techniques for determination of polymer solution viscosity in the presence of SiO_2 nanoparticle and salinity. *Spectrochim. Acta A Mol. Biomol. Spectrosc.* 220, 117049. https://doi.org/10.1016/j.saa.2019.04.041.

Naushad, M., Khan, M.R., ALOthman, Z.A., AlSohaimi, I., Rodriguez-Reinoso, F., Turki, T.M., Ali, R. (2015). Removal of BrO_3-from drinking water samples using newly developed agricultural waste-based activated carbon and its determination by ultra-performance liquid chromatography-mass spectrometry. *Environ. Sci. Pollut. Res.* 22 (20), 15853-15865. https://doi.org/10.1007/s11356-015-4786-y.

Nicasio-Collazo, J., Ramírez-García, G., Flores-Álamo, M., Gutiérrez-Granados, S., Peralta-Hernández, J.M., Maldonado, J.L., Oscar, J., Jimenez-Halla, C., Serrano, O. (2019). A novel coordination mode of κ^1-N-Br-pyridylbenz-(imida, oxa or othia)-zole to $Pt_{(II)}$: synthesis, characterization, electrochemical and structural analysis. *RSC Adv.* 9 (25), 14033-14039. https://doi.org/10.1039/c9ra01856e.

Oberdörster, G., Maynard, A., Donaldson, K., Castranova, V., Fitzpatrick, J., Ausman, K., Karn, B., Kreyling, W., Lai, D., Olin, S., Warheti, D., Yang, H. (2005). Principles for characterizing the potential human health effects from exposure to nanomaterials: elements of a screening strategy. *Part. Fibre Toxicol.* 2 (1), 1-35. https://doi.org/10.1186/1743-8977-2-8.

Oswald, S., Suhm, M.A., Coussan, S. (2019). Incremental NH stretching downshift through stepwise nitrogen complexation of pyrrole: a combined jet expansion and matrix isolation study. *Phys. Chem. Chem. Phys.* 21 (3), 1277-1284. https://doi.org/10.1039/C8CP07053A.

Palmer, W.G., Eaton, J.C. (2001). *Effects of Welding on Health, XIV*. American Welding Society, pp. 1-66.

Panja, A., Ghosh, K. (2019). Cholesterol-based simple supramolecular gelators: an approach to selective sensing of CN- ion with application in dye adsorption. *Supramol. Chem.* 31 (4), 239-250. https://doi.org/10.1080/10610278.2018.1562190.

Ponmudi, S., Sivakumar, R., Sanjeeviraja, C., Gopalakrishnan, C., Jeyadheepan, K. (2019). Tuning the morphology of Cr_2O_3: CuO (50:50) thin films by RF magnetron sputtering for room temperature sensing application. *Appl. Surf. Sci.* 466, 703-714. https://doi.org/10.1016/j.apsusc.2018.10.096.

Rana, H.K., Akhtar, M.R., Islam, M.B., Ahmed, M.B., Lio, P., Quinn, J.M., Moni, M.A. (2019). Genetic effects of welding fumes on the development of respiratory system diseases. *Comput. Biol. Med.* 108, 142-149. https://doi.org/10.1016/j.compbiomed.2019.04.004.

Reddy, G.K., Peck, T.C., Roberts, C.A. (2019). "PdO vs. PtO"-The Influence of PGM Oxide Promotion of Co_3O_4 Spinel on Direct NO Decomposition Activity. *Catalysts* 9 (1). 1-18. https://doi.org/10.3390/catal9010062.

Sahai, A., Goswami, N., Kaushik, S.D., Tripathi, S. (2016). $Cu/Cu_2O/CuO$ nanoparticles: Novel synthesis by exploding wire technique and extensive characterization. *Appl. Surf. Sci.* 390, 974-983. https://doi.org/10.1016/j.apsusc.2016.09.005.

Saikia, B.J., Parthasarathy, G. (2010). Fourier transform infrared spectroscopic characterization of kaolinite from Assam and Meghalaya, Northeastern India. *J. Mod. Phys.* 1 (4), 206-210. https://doi.org/10.4236/jmp.2010.14031.

Scaccia, S., Vanga, G., Gattia, D.M., Stendardo, S. (2019). Preparation of CaO-based sorbent from coal fly ash cenospheres for calcium looping process. *J. Alloy. Compd.* 801, 123-129. https://doi.org/10.1016/j.jallcom.2019.06.064.

Sevilla, M., Fuertes, A.B. (2009). Chemical and structural properties of carbonaceous products obtained by hydrothermal carbonization of saccharides. *Chem. Eur. J.* 15 (16), 4195-4203. https://doi.org/10.1002/chem.200802097.

Shackelford, J.F., Han, Y.H., Kim, S., Kwon, S.H. (2016). *Metals*. In *CRC Materials Science and Engineering Handbook*. CRC press, pp. 25-40.

Sjogren, B., Gyntelberg, F., Hilt, B. (2006). Ischemic heart disease and welding in Scandinavian studies. *Scand. J. Work Env. Hea.* 2 (2), 50-53.

Sowards, J.W., Ramirez, A.J., Lippold, J.C., Dickinson, D.W. (2008). Characterization procedure for the analysis of arc welding fume. *Weld. J.* 87 (3), 76-83.

Sowards, J. W., Ramirez, A. J., Dickinson, D. W., Lippold, J.C. (2010). Characterization of welding fume from SMAW electrodes-Part II. *Weld. J.* 89, 82-90.

Stebounova, L.V., Gonzalez-Pech, N.I., Peters, T.M., Grassian, V.H. (2018). Physicochemical properties of air discharge-generated manganese oxide nanoparticles: comparison to welding fumes. *Environ. Sci.: Nano* 5 (3), 696-707. https://doi.org/10.1039/c7en01046j.

Stockmann-Juvala, H., Hedberg, Y., Dhinsa, N.K., Griffiths, D.R., Brooks, P.N., Zitting, A., Odnevall Wallinder, I., Santonen, T. (2013). Inhalation toxicity of 316L stainless steel powder in relation to bioaccessibility. *Hum. Exp. Toxicol.* 32 (11), 1137-1154. https://doi.org/10.1177/0960327112472354.

Turan, E., Koçal, T., Ünlügençoğlu, K. (2011). Welding technologies in shipbuilding industry. *TOJSAT* 1 (4), 24-31.

Vaculikova, L., Plevová, E., Vallová, S., Koutnik, I. (2011). Characterization and differentiation of kaolinites from selected Czech deposits using infrared spectroscopy and differential thermal analysis. *Acta Geodyn. Geomater.* 8 (1), 59-67.

Wang, H., Yu, M., Lin, C.K., Lin, J. (2006). Core–shell structured SiO_2@ YVO_4: Dy^{3+}/Sm^{3+} phosphor particles: sol–gel preparation and characterization. *J. Colloid Interf. Sci.* 300 (1), 176-182. https://doi.org/10.1016/j.jcis.2006.03.052.

Wang, S., Zhou, S., Huang, J., Zhao, G., Liu, Y. (2019a). Attaching ZrO_2 nanoparticles onto the surface of graphene oxide via electrostatic self-assembly for enhanced mechanical and tribological performance of phenolic resin composites. *J. Mater. Sci.* 54 (11), 8247-8261. https://doi.org/10.1007/s10853-019-03512-w.

Wang, S., Wu, S.H., Fang, W.L., Guo, X.F., Wang, H. (2019b). Synthesis of non-doped and non-modified carbon dots with high quantum yield and crystallinity by one-pot hydrothermal method using a single carbon source and used for ClO^- detection. *Dyes Pigm.* 164, 7-13. https://doi.org/10.1016/j.dyepig.2019.01.004.

Yang, K., Yi, H., Tang, X., Zhao, S., Gao, F., Huang, Y., Yang, Z., Wang, J., Shi, Y., Xie, X. (2019). Reducing the competitive adsorption between SO_2 and NO by Al_2O_3@TiO_2 core-shell structure adsorbent. *Chem. Eng. J.* 364, 420-427. https://doi.org/10.1016/j.cej.2019.02.009.

Yi, H., Yang, K., Tang, X., Zhao, S., Gao, F., Huang, Y., Yang, Z., Wang, Y., Xie, X. (2018). Simultaneous Desulfurization and Denitrification on the SAPO-34@Al_2O_3 Core–Shell Structure Adsorbent. *Energy Fuels* 32 (11), 11694-11700. https://doi.org/10.1021/acs.energyfuels.8b02847.

Zheng, M., Liu, Y., Jiang, K., Xiao, Y., Yuan, D. (2010). Alcohol-assisted hydrothermal carbonization to fabricate spheroidal carbons with a tunable shape and aspect ratio. *Carbon* 48 (4), 1224-1233. https://doi.org/10.1016/j.carbon.2009.11.045.